Article

Carbon dioxide capture from open air using covalent organic frameworks

https://doi.org/10.1038/s41586-024-08080-x

Received: 29 April 2024

Accepted: 17 September 2024

Published online: 23 October 2024

Check for updates

Zihui Zhou[1,2,3,4], Tianqiong Ma[1,2,3,4], Heyang Zhang[1,2,3,4], Saumil Chheda[1,2,3,4], Haozhe Li[1,2,3,4], Kaiyu Wang[1,2,3,4], Sebastian Ehrling[5], Raynald Giovine[1], Chuanshuai Li[1,2,3,4], Ali H. Alawadhi[1,2,3,4], Marwan M. Abduljawad[4], Majed O. Alawad[4], Laura Gagliardi[6], Joachim Sauer[7] ✉ & Omar M. Yaghi[1,2,3,4] ✉

Capture of CO_2 from the air offers a promising approach to addressing climate change and achieving carbon neutrality goals[1,2]. However, the development of a durable material with high capacity, fast kinetics and low regeneration temperature for CO_2 capture, especially from the intricate and dynamic atmosphere, is still lacking. Here a porous, crystalline covalent organic framework (COF) with olefin linkages has been synthesized, structurally characterized and post-synthetically modified by the covalent attachment of amine initiators for producing polyamines within the pores. This COF (termed COF-999) can capture CO_2 from open air. COF-999 has a capacity of 0.96 mmol g^{-1} under dry conditions and 2.05 mmol g^{-1} under 50% relative humidity, both from 400 ppm CO_2. This COF was tested for more than 100 adsorption–desorption cycles in the open air of Berkeley, California, and found to fully retain its performance. COF-999 is an exceptional material for the capture of CO_2 from open air as evidenced by its cycling stability, facile uptake of CO_2 (reaches half capacity in 18.8 min) and low regeneration temperature (60 °C).

Efficient capture of CO_2 from air requires a material to be selective, have a high capacity for CO_2 and exhibit fast kinetics—all under low CO_2 concentration (around 400 ppm). Furthermore, this material must be operated with low regeneration temperature and high cycling stability in the presence of other air components, especially oxygen and water[3–5]. Extensive research has been reported for using liquid alkaline solutions[6,7], metal–organic frameworks (MOFs)[8–12] and silica-supported amines[13–15] as potential candidates for direct air capture (DAC) application (see Supplementary Tables 1 and 2 for more details). However, despite their promise, the full deployment of liquid solutions has been challenged by their energy-intensive regeneration[3] and toxicity, whereas for MOFs and silica-supported amines, hydrolysis[16,17] and loss of amines[18] on cycling remain persistent problems. Using the design principles of reticular chemistry[19,20], amine-functionalized covalent organic frameworks (COFs)[21] were synthesized to increase CO_2 physisorption affinity for the separation of CO_2 from gas mixtures (typical CO_2 concentration greater than 10%). However, to capture CO_2 directly from the air under practical conditions, it is essential to incorporate stronger chemisorption sites[4,22] in a more stable backbone. In this study, we designed a porous, crystalline COF (termed COF-999) that selectively captures 2.05 mmol of CO_2 per gram sorbent from air containing 400 ppm of CO_2 at 50% relative humidity (RH). We show the cycling stability of this COF by performing 100 CO_2 adsorption–desorption temperature-swing cycles (ambient temperature to 60 °C) over 20 days of operation in the open air, with full retention of its capacity and performance. COF-999 exceeds the current state-of-the-art materials in DAC application, and COF chemistry, in general, presents extensive opportunities for molecular design and ultimately deployment of this emerging class of materials.

Our strategy is outlined in Fig. 1, in which the molecular attributes needed to address the DAC challenges are incorporated into the COF. First, the use of hydrophobic building units in the construction of the COF provides for hydrophobic pores into which a minimum amount of water could be adsorbed, leading to a lower CO_2 regeneration temperature[22–24]. Second, the initiators are covalently bound to the framework and, in turn, allow the covalent attachment of polyamines and prevent their loss during cycling. The fact that the initiators are designed to be reactive and the pores are intentionally large provides for opportunities to have a high loading of polyamines and facile diffusion of CO_2—necessary prerequisites for achieving high capacity and rapid cycling. Third, the olefin linkage between covalent molecules making up the COF backbone leads to the overall thermal and chemical stability of the structure[25,26] to allow the post-synthetic installation of the polyamine units and repeated CO_2 cycling stability without compromising the porosity and integrity of the COF structure.

Synthesis and structure of the COF series

A porous, crystalline olefin-linked COF precursor, COF-999-N_3, was first synthesized through Knoevenagel condensation between 3,3′-bis[(6-azidohexyl)oxy]-4,4′-biphenyldicarbaldehyde (BPDA-N_3) and 1,3,5-tris(4-cyanomethylphenyl)benzene (TCPB) (Fig. 1). Powder X-ray diffraction (PXRD) measurement was carried out to confirm the crystallinity of COF-999-N_3 (Fig. 2a). Pawley refinement[27] was conducted

[1]Department of Chemistry, University of California, Berkeley, CA, USA. [2]Kavli Energy NanoScience Institute, University of California, Berkeley, CA, USA. [3]Bakar Institute of Digital Materials for the Planet, College of Computing, Data Science, and Society, University of California, Berkeley, CA, USA. [4]KACST-UC Berkeley Center of Excellence for Nanomaterials for Clean Energy Applications, King Abdulaziz City for Science and Technology, Riyadh, Saudi Arabia. [5]3P Instruments, Leipzig, Germany. [6]Department of Chemistry, Pritzker School of Molecular Engineering, and Chicago Center for Theoretical Chemistry, University of Chicago, Chicago, IL, USA. [7]Institut für Chemie, Humboldt-Universität zu Berlin, Berlin, Germany. ✉e-mail: js@chemie.hu-berlin.de; yaghi@berkeley.edu

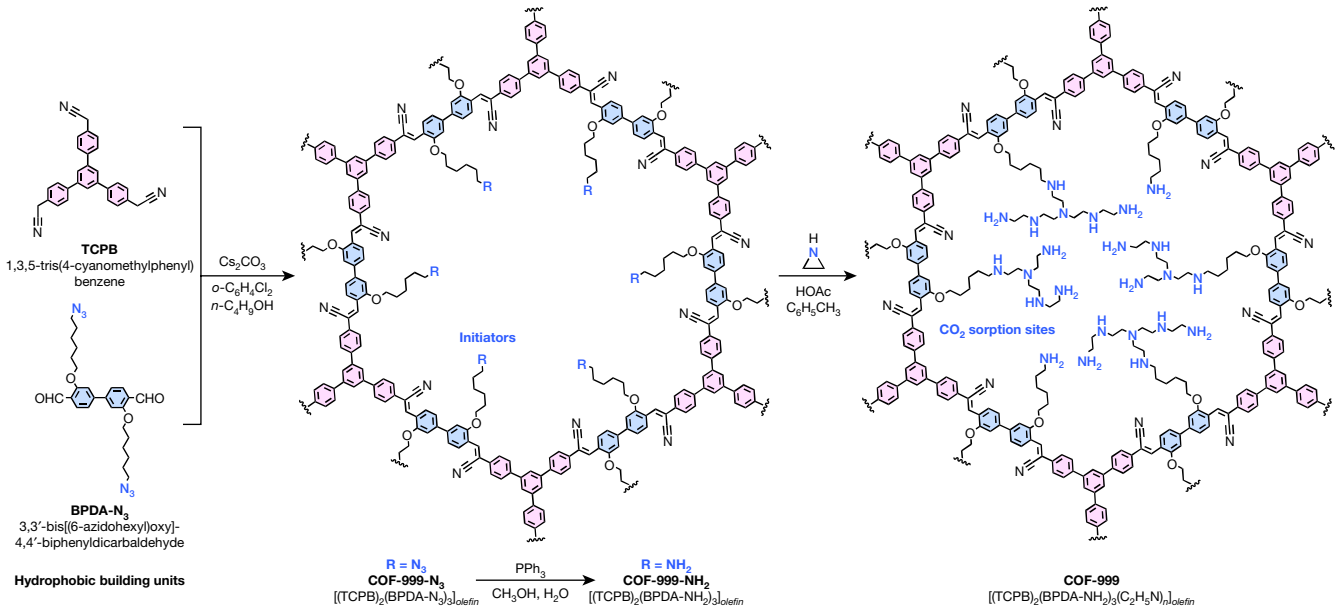

Fig. 1 | Design strategy and synthesis of COF-999. The condensation reaction between BPDA-N_3 and TCPB results in COF-999-N_3, followed by the reduction of azides to form COF-999-NH_2. The reactive amine initiators mounted on the backbone allow for the covalent installation of polyamines through a ring-opening polymerization reaction with aziridine, yielding COF-999.

with the experimental PXRD pattern of COF-999-N_3 in the space group of *P*6 to yield unit cell parameters of $a = b = 45.524(2)$ Å, $c = 3.94(9)$ Å, $\alpha = \beta = 90°$ and $\gamma = 120°$ with profile residual factor $R_p = 1.81\%$ and weighted profile residual factor $R_{wp} = 3.12\%$. The PXRD peaks at 2.2°, 3.9°, 4.5°, 5.9° and 6.7° were assigned to the (100), (110), (200), (210) and (300) lattice planes, respectively. These observations are consistent with the simulated structure, in which BPDA-N_3 and TCPB are connected through olefin linkages to form honeycomb sheets with AA stacking. Scanning electron microscopy (SEM) image of COF-999-N_3 showed a textured spherically shaped morphology with an average particle size of 5 µm (Supplementary Fig. 1). The N_2 sorption isotherm of COF-999-N_3 was measured at 77 K (Fig. 2b), giving a Brunauer–Emmett–Teller surface area[28] of 811 $m^2 g^{-1}$, with an average pore size of 3.3 nm (Supplementary Fig. 2). The azide functional groups within the pore were characterized by ^{15}N cross-polarization magic-angle spinning (CP-MAS) solid-state nuclear magnetic resonance (ssNMR) using ^{15}N-labelled COF-999-$^{15}N_3$ (Fig. 2c). Two dominant peaks at 210.4 ppm and 71.6 ppm were attributed to labelled γ-^{15}N (R–N=N=*N) and α-^{15}N (R–*N=N=N) on the azide groups of the sidechain.

Further reduction of its azide groups to amines by Staudinger reaction[29] under room temperature afforded COF-999-NH_2, which was then treated with aziridine to produce polyamines within the pore to obtain COF-999 (Fig. 1). ^{15}N ssNMR spectra were collected to prove the conversion of azide to amine to polyamine (Fig. 2c). The complete reduction of COF-999-$^{15}N_3$ was confirmed by the disappearance of the azide peaks and the emergence of characteristic R–$^{15}NH_2$ chemical shift[30] at 23.5 ppm in ^{15}N ssNMR spectra. This can also be monitored by the absence of vibrational absorbance bands at 2,089 cm^{-1} for azide $\nu_{N=N}$ stretch[29] from Fourier-transform infrared (FT-IR) spectroscopy (Supplementary Fig. 9). Notably, the crystallinity and porosity of COF-999-NH_2 were retained upon performing the reduction process (Supplementary Figs. 3 and 11). The in-pore polymerization of COF-999-$^{15}NH_2$ with unlabelled aziridine gave a new peak at 35.7 ppm in the ^{15}N ssNMR spectrum of COF-999, which was assigned to the formation of secondary amines[30] connecting the COF backbone and polyethylenimine units. Quantitative ^{15}N multiple-CP-MAS (multiCP-MAS) ssNMR showed that 66% of the primary amines on the side chains (COF-999-NH_2, Fig. 1) were converted to secondary amines (COF-999, Fig. 1) upon polymerization (see Supplementary Fig. 14 for details). The degree of polymerization for COF-999 was calculated from quantitative ^{13}C multiCP-MAS ssNMR (Fig. 2d) and elemental analysis (Supplementary Table 6), indicating an average of 4.6 CH_2CH_2NH units were added to each reacted amine side chain (Supplementary Information section 9).

Gas sorption isotherms

We initially examined the uptake of air components by COF-999 through gas sorption isotherm measurements for CO_2, N_2, O_2, Ar and H_2O at 25 °C (Fig. 3a–c). A steep increase at very low CO_2 pressures was observed (Fig. 3a), as well as the hysteresis between the adsorption and desorption isotherms, indicating the strong affinity of COF-999 for CO_2. From these data, we found that the uptake for CO_2 is 0.91 mmol g^{-1} at 0.4 mbar (400 ppm, condition close to the CO_2 partial pressure in air, Fig. 3b), and the corresponding calculated isosteric heat of adsorption is 53 kJ mol^{-1} (Supplementary Fig. 6). As expected, N_2, O_2 and Ar exhibited linear-shaped sorption isotherms with negligible uptake (Fig. 3a), indicating that COF-999 possesses a high selectivity for CO_2 over other components present in ambient air. The water uptake of COF-999 was 0.09 $g_{water}\ g_{COF}^{-1}$ at 50% RH (Fig. 3c), with an isosteric heat of water vapour adsorption of 49 kJ mol^{-1} (Supplementary Fig. 8). This low water uptake has positive implications for CO_2 capture from air by this material as discussed further below.

Kinetic uptake of gas from mixtures

Multicomponent breakthrough experiments enable the assessment of sorption selectivity and dynamic behaviour (Fig. 3d–i), which are important for evaluating the practical performance of the sorbent in air. Given that oxygen and water are the main components in the atmosphere, any candidate material for carbon capture must be stable under humid and oxidizing conditions. Dynamic sorption curves were measured under 400 ppm of CO_2 balanced in synthetic air (N_2:O_2 = 4:1 volume ratio) with 50% RH at 25 °C to simulate ambient conditions (Fig. 3d). COF-999 adsorbed both CO_2 and water after being exposed to the simulated air (400 ppm of CO_2 with 50% RH). Initially, the material quickly reached the saturated capacity for water adsorption compared with CO_2, which was retained in the pores before it broke through at approximately 90 min with a steep concentration increase. COF-999

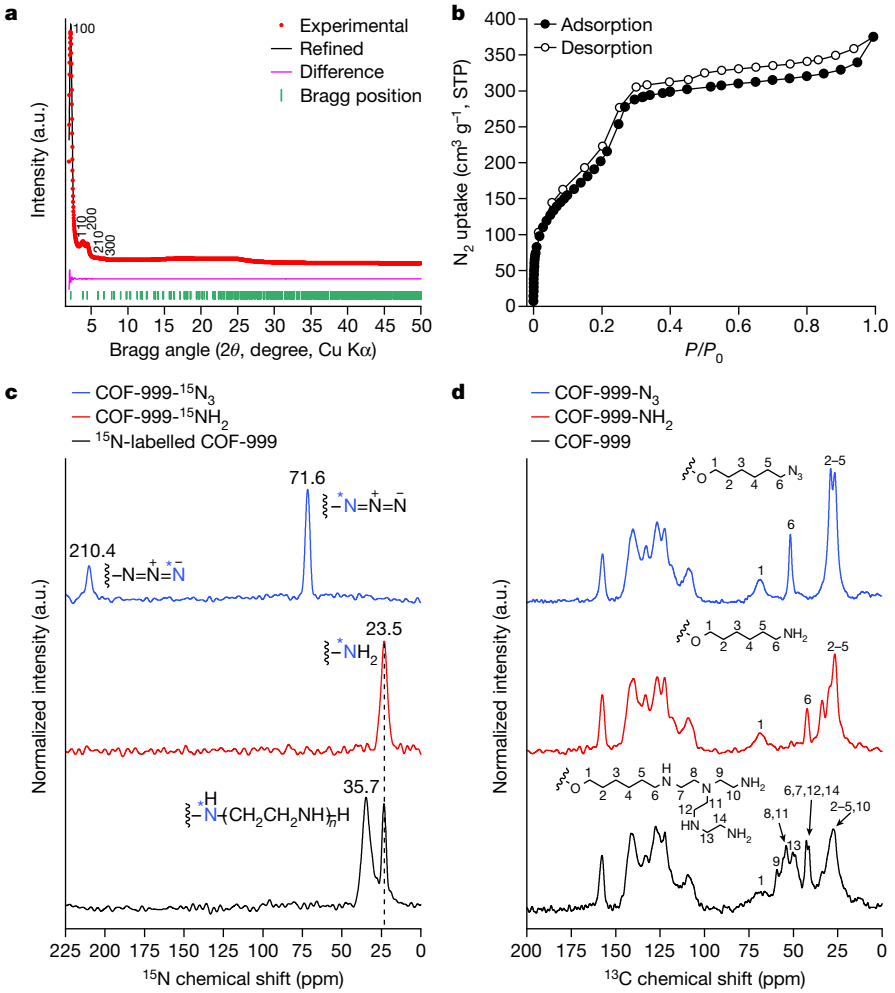

Fig. 2 | Characterization of COF-999 series. a, Experimental PXRD pattern (red), Pawley refined pattern (black), difference pattern (pink) and Bragg positions (green) of COF-999-N_3. **b**, N_2 sorption isotherm of COF-999-N_3 measured at 77 K. *P*, nitrogen pressure; P_0 = 1 atm; STP, standard temperature and pressure. **c**, Comparison of ^{15}N CP-MAS ssNMR spectra of COF-999-$^{15}N_3$ (blue) and COF-999-$^{15}NH_2$ (red), and quantitative ^{15}N multiCP-MAS ssNMR spectrum of ^{15}N-labelled COF-999 (black). ^{15}N-labelled nitrogen atoms are marked with asterisks. Signals from unlabelled nitrogen (aziridine and nitrile) can be neglected because of their low natural abundance. **d**, Comparison of ^{13}C CP-MAS ssNMR spectrum of COF-999-N_3 (blue) and quantitative ^{13}C multiCP-MAS ssNMR spectra of COF-999-NH_2 (red) and COF-999 (black). a.u., arbitrary units.

eventually reached the equilibrium concentration with CO_2, indicating the saturated adsorption capacity was reached. The sharp breakthrough curve suggests the rapid mass transfer[31] of CO_2 in COF-999.

The impact of water on CO_2 adsorption was evaluated by measuring the CO_2 uptake of COF-999 under varying RH levels from 0% to 75% at 25 °C (Fig. 3e and Supplementary Fig. 16). The cumulative CO_2 uptakes were calculated through numerical integration of the CO_2 concentration differences between the backgrounds and the monitored downstream concentrations. Under dry conditions with 400 ppm of CO_2, COF-999 exhibited a CO_2 uptake of 0.96 ± 0.03 mmol g^{-1}, which is comparable to its single-component CO_2 sorption result. When 25% RH was introduced into the measurement, the CO_2 adsorption capacity of COF-999 increased to 1.69 ± 0.08 mmol g^{-1}. A further increase to 2.05 ± 0.03 mmol g^{-1} in the capacity was observed on increasing RH to 50%. This is a remarkable 2.14-fold increase in CO_2 capacity over the dry condition. A maximum capacity of 2.09 ± 0.03 mmol g^{-1} was achieved at 75% RH. The marked positive impact of water on CO_2 uptake is because of the formation of carbamates and bicarbonates in the pores shown by ssNMR measurements (Supplementary Fig. 26) and explained by density functional theory calculations (Supplementary Information section 14) presented below. Although not the emphasis of this contribution, under simulated natural-gas flue gas (4% of CO_2 with 75% RH) and coal flue gas (15% of CO_2 with 75% RH) conditions, the CO_2 uptake capacity of COF-999 was found to be 3.17 mmol g^{-1} and 3.24 mmol g^{-1}, respectively (Supplementary Figs. 18 and 19), indicating the CO_2 capture ability of COF-999 under various working conditions.

The adsorption kinetics of COF-999 was measured under simulated air (400 ppm of CO_2 with 50% RH) at 25 °C (Fig. 3f and Supplementary Fig. 20). Specifically, the COF reached half capacity (1.01 mmol g^{-1}) within 18.8 min and 80% capacity (1.62 mmol g^{-1}) within 61.7 min. During the adsorption process, the maximum adsorption rate was calculated as 0.11 mmol g^{-1} min^{-1}. This ultrafast rate is the highest measured for CO_2 capture from air, to our knowledge, albeit the reported measurements were done under dry conditions[32]. We attribute our facile adsorption not only to the periodic pore structure of COF-999 but also to the presence of a small amount of water within the pore[33].

To investigate the impact of desorption temperature on desorption kinetics, we measured the desorption kinetics curves at 60 °C, 80 °C and 100 °C (Fig. 3g,h and Supplementary Fig. 21). Before the measurement, COF-999 was saturated with simulated air (400 ppm of CO_2 with 50% RH) at 25 °C. The temperature was then ramped up within 5 min and maintained under nitrogen flow. At 60 °C, 44.1 min was needed to desorb 80% of the adsorbed CO_2, and the maximum desorption rate was calculated to be 0.06 mmol g^{-1} min^{-1}. Increasing

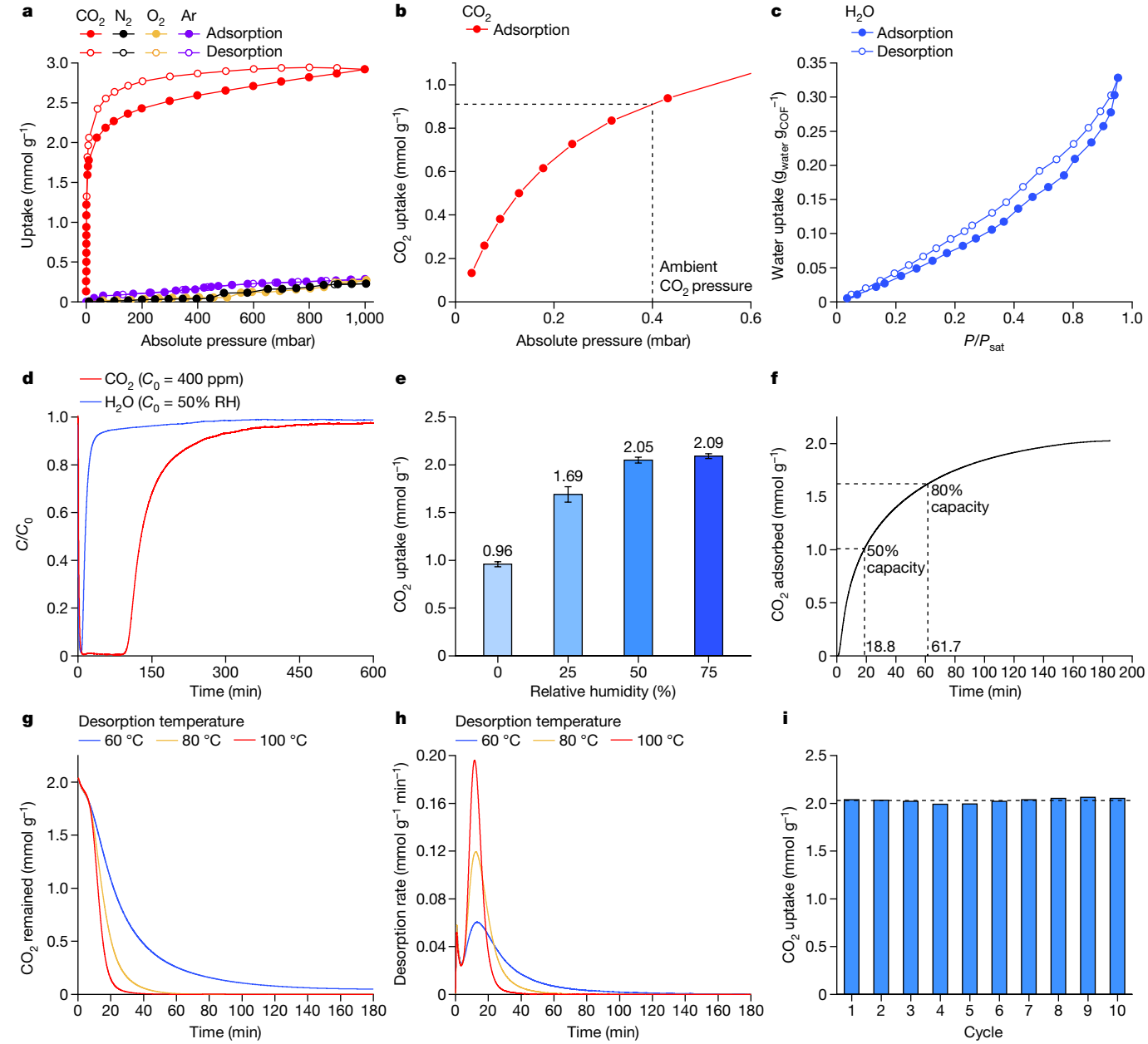

Fig. 3 | Thermodynamic and kinetic gas sorption studies of COF-999. **a**, Comparison of single-component CO_2 (red), N_2 (black), O_2 (yellow) and Ar (violet) sorption isotherms measured at 25 °C. **b**, Magnified view of the CO_2 sorption isotherm taken from **a** highlighting the uptake at the ambient CO_2 pressure (0.4 mbar). **c**, Single-component H_2O vapour sorption isotherm measured at 25 °C, for which P is water vapour pressure and P_{sat} is the saturation water vapour pressure. **d**, CO_2 (red) and H_2O (blue) breakthrough curves under humid simulated air (400 ppm of CO_2 with 50% RH) at 25 °C. C and C_0 represent adsorbate concentration in the downstream and upstream gas flow, respectively. **e**, CO_2 uptake under 400 ppm of CO_2 with 0%, 25%, 50% and 75% RH. The data shown are statistical averages and the error bars represent 1 standard deviation. **f**, CO_2 adsorption kinetics curve under humid simulated air (400 ppm of CO_2 with 50% RH) at 25 °C. **g**, Comparison of CO_2 desorption kinetics curves at 60 °C (blue), 80 °C (yellow) and 100 °C (red). **h**, Comparison of CO_2 desorption rates at 60 °C (blue), 80 °C (yellow) and 100 °C (red). **i**, CO_2 uptake under humid simulated air (400 ppm of CO_2 with 50% RH) at 25 °C derived from 10 temperature-swing cycling breakthrough measurements, giving an average working capacity of 2.03 mmol g^{-1} (dotted line).

the temperature to 80 °C resulted in a higher maximum desorption rate of 0.12 mmol g^{-1} min^{-1}; and at 21.8 min, 80% of the adsorbed CO_2 was desorbed. Further elevating the temperature to 100 °C yielded a maximum desorption rate of 0.19 mmol g^{-1} min^{-1}, with 80% of the adsorbed CO_2 desorbed in 15.9 min. The hydrophobic nature of COF-999 allows CO_2 desorption with lower energy input for the removal of water molecules (Supplementary Information section 12), thereby resulting in a low desorption temperature and fast desorption kinetics.

An initial assessment of the cycling stability of COF-999 was done by a temperature-swing measurement in simulated air (400 ppm of CO_2 with 50% RH). The COF sample was regenerated under 60 °C in nitrogen flow after each cycle. The retention of CO_2 capacity after 10 consecutive adsorption–desorption cycles showed excellent stability of COF-999 (Fig. 3i and Supplementary Fig. 23).

Carbon dioxide capture from open air

The viability of COF-999 under practical conditions was tested in outdoor air by conducting the experiment continuously for 20 days in Berkeley, California, United States (37° 52′ 23.8″ N, 122° 15′ 21.2″ W),

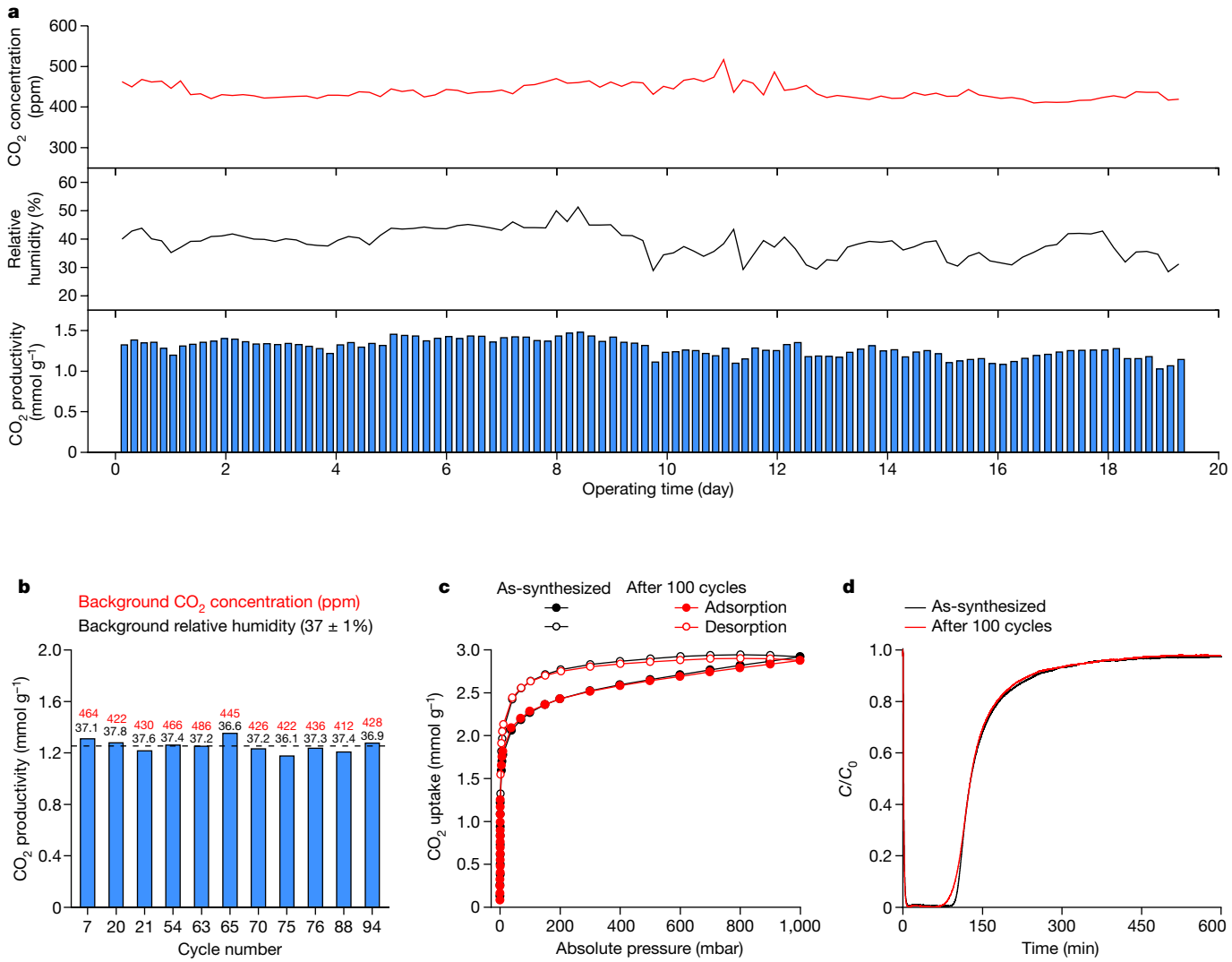

Fig. 4 | Carbon dioxide capture from open air. a, CO_2 capture productivity after each adsorption cycle (blue), corresponding ambient outdoor CO_2 concentration (red) and RH (black). All data were measured for 20 continuous days of operation using outdoor air. **b**, CO_2 productivity of selected cycles with an ambient RH of 37 ± 1%, with corresponding ambient outdoor CO_2 concentration. The average productivity of selected cycles is shown as the dotted line. **c**, Comparison of single-component CO_2 sorption isotherms (25 °C) of as-synthesized COF-999 and the sample after 100 outdoor air cycles. **d**, Comparison of CO_2 breakthrough curves using simulated air (400 ppm of CO_2 with 50% RH) at 25 °C run on as-synthesized COF-999 and the sample after 100 outdoor air cycles. C and C_0 represent adsorbate concentrations in the downstream and upstream gas flow, respectively.

from 18 January 2024 to 6 February 2024 (Fig. 4a and Supplementary Information section 11). Outdoor air was passed through the sorbent, in which CO_2 molecules were selectively adsorbed by COF-999. The breakthrough point of the adsorption process was set to be 300 ppm downstream because this represents most of the CO_2 adsorbed. Then, the material was regenerated at 60 °C. In this measurement approach, it is possible to run a higher number of cycles and to assess the adsorption–desorption cycling performance, while operating at near-full capacity. Throughout the experiment, the ambient outdoor CO_2 concentration and RH were measured before each adsorption process.

One hundred adsorption–desorption cycles were performed over the 20 days during which outdoor CO_2 concentration varied from 410 ppm to 517 ppm and the RH from 28% to 51%. The average CO_2 productivity was determined to be 1.28 mmol g^{-1} per cycle (5.63 wt% per cycle) over 100 consecutive cycles, with a maximum productivity of 1.48 mmol g^{-1} and minimum productivity of 1.03 mmol g^{-1}. We observed that as the humidity in the air varies over time, the enhancement of CO_2 uptake also varies (Fig. 4a). This positive impact of humidity on CO_2 uptake is rooted in the manner with which water molecules interact with the CO_2 bound to the amines as elaborated below. The CO_2 productivities of cycles with a background of 37 ± 1% RH were plotted to demonstrate the stability of COF-999 under these varying open-air conditions (Fig. 4b). The chemical robustness of the COF is supported by the consistent capacity found for those cycles carried out under the same humidity. We further measured single-component CO_2 sorption isotherm (Fig. 4c), dynamic breakthrough using simulated air (400 ppm of CO_2 with 50% RH) (Fig. 4d), FT-IR (Supplementary Fig. 10) and SEM (Supplementary Fig. 1) of COF-999 after the completion of the 100 adsorption–desorption cycles. No changes in sorption isotherm, breakthrough, FT-IR and SEM were observed, indicating retention of the COF structure and its proper functioning in CO_2 capture.

Adsorption structures of CO_2 in COF-999

^{13}C ssNMR spectroscopy was used to study the binding of CO_2 molecules by COF-999 (Supplementary Fig. 26). On exposing COF-999 to 1 atm $^{13}CO_2$ at 25 °C under dry conditions, we observed an intense signal at 164.5 ppm in the ^{13}C spectrum, which we assign to the formation of carbamic acid as the result of CO_2 reacting with the polyamines[30,34]. By contrast, pre-saturation with water of COF-999 at 80% RH in N_2 at

25 °C, followed by exposure to $^{13}CO_2$, led to the appearance of signals at 165.1 ppm and 161.7 ppm in the ^{13}C spectrum, indicating the formation of carbamate and bicarbonate, respectively.

Periodic density functional theory calculations of the CO_2 adsorption structures in the COF (Supplementary Information section 14) suggested that under dry conditions, the reaction between CO_2 and primary or secondary amines is energy favoured, and the formed carbamic acid is stabilized by hydrogen bonds with adjacent amines (for example, Extended Data Fig. 1a, N···O distance of 263 pm). On addition of water molecules, we found that the formed carbamic acid and carbamate are stabilized through hydrogen bonds (for example, Extended Data Fig. 1b, O···O_w distance of 283 pm and N···O distance of 257 pm) and promoted the formation of bicarbonates, which are also stabilized by hydrogen bonds with adjacent amine groups (for example, Extended Data Fig. 1c, N···O distances of 262 ppm and 271 ppm). Thus, the stabilization in the presence of water explains the experimentally observed marked enhancement of CO_2 uptake by COF-999 under humid conditions and its suitability for open-air CO_2 capture.

Outlook

We have shown how COFs with an olefin-linked backbone and covalently attached sorption sites, bringing ultrahigh chemical stability, can serve as excellent materials for capturing CO_2 from the air. Our studies demonstrate that this application in the open air is a marked advance towards achieving clean air. It is also clear that the present COF-999 is perhaps one of the first members of what we believe will be a large class of materials with a robust framework backbone that we expect will serve the general purpose of carbon capture very well. By applying this strategy, other reticular structures will have to be designed, examined and compared with COF-999 to further improve the capacity and performance. In the meantime, the scalability of this COF and the design of a practical device will be an important priority for future implementation of these materials.

Online content

Any methods, additional references, Nature Portfolio reporting summaries, source data, extended data, supplementary information, acknowledgements, peer review information; details of author contributions and competing interests; and statements of data and code availability are available at https://doi.org/10.1038/s41586-024-08080-x.

1. Lackner, K., Ziock, H.-J. & Grimes, P. Carbon dioxide extraction from air: is it an option? in *24th Annual Technical Conference on Coal Utilization and Fuel Systems* (Clearwater, 1999).
2. Lackner, K. S. et al. The urgency of the development of CO_2 capture from ambient air. *Proc. Natl Acad. Sci. USA* **109**, 13156–13162 (2012).
3. Sanz-Pérez, E. S., Murdock, C. R., Didas, S. A. & Jones, C. W. Direct capture of CO_2 from ambient air. *Chem. Rev.* **116**, 11840–11876 (2016).
4. Shi, X. et al. Sorbents for the direct capture of CO_2 from ambient air. *Angew. Chem. Int. Ed.* **59**, 6984–7006 (2020).
5. Zhu, X. et al. Recent advances in direct air capture by adsorption. *Chem. Soc. Rev.* **51**, 6574–6651 (2022).
6. Brethomé, F. M., Williams, N. J., Seipp, C. A., Kidder, M. K. & Custelcean, R. Direct air capture of CO_2 via aqueous-phase absorption and crystalline-phase release using concentrated solar power. *Nat. Energy* **3**, 553–559 (2018).
7. Keith, D. W., Holmes, G., St. Angelo, D. & Heidel, K. A process for capturing CO_2 from the atmosphere. *Joule* **2**, 1573–1594 (2018).
8. Shekhah, O. et al. Made-to-order metal-organic frameworks for trace carbon dioxide removal and air capture. *Nat. Commun.* **5**, 4228 (2014).
9. McDonald, T. M. et al. Capture of carbon dioxide from air and flue gas in the alkylamine-appended metal-organic framework mmen-Mg_2(dobpdc). *J. Am. Chem. Soc.* **134**, 7056–7065 (2012).
10. Bien, C. E. et al. Bioinspired metal-organic framework for trace CO_2 capture. *J. Am. Chem. Soc.* **140**, 12662–12666 (2018).
11. Chen, O. I.-F. et al. Water-enhanced direct air capture of carbon dioxide in metal-organic frameworks. *J. Am. Chem. Soc.* **146**, 2835–2844 (2024).
12. Nugent, P. et al. Porous materials with optimal adsorption thermodynamics and kinetics for CO_2 separation. *Nature* **495**, 80–84 (2013).
13. Deutz, S. & Bardow, A. Life-cycle assessment of an industrial direct air capture process based on temperature–vacuum swing adsorption. *Nat. Energy* **6**, 203–213 (2021).
14. Miao, Y., He, Z., Zhu, X., Izikowitz, D. & Li, J. Operating temperatures affect direct air capture of CO_2 in polyamine-loaded mesoporous silica. *Chem. Eng. J.* **426**, 131875 (2021).
15. Rim, G., Feric, T. G., Moore, T. & Park, A. H. A. Solvent impregnated polymers loaded with liquid-like nanoparticle organic hybrid materials for enhanced kinetics of direct air capture and point source CO_2 capture. *Adv. Funct. Mater.* **31**, 2010047 (2021).
16. Choe, J. H. et al. Boc protection for diamine-appended MOF adsorbents to enhance CO_2 recyclability under realistic humid conditions. *J. Am. Chem. Soc.* **146**, 646–659 (2024).
17. Barsoum, M. L. et al. Probing structural transformations and degradation mechanisms by direct observation in SIFSIX-3-Ni for direct air capture. *J. Am. Chem. Soc.* **146**, 6557–6565 (2024).
18. Carneiro, J. S. A. et al. Insights into the oxidative degradation mechanism of solid amine sorbents for CO_2 capture from air: roles of atmospheric water. *Angew. Chem. Int. Ed.* **62**, e2023028 (2023).
19. Yaghi, O. M., Kalmutzki, M. J. & Diercks, C. S. *Introduction to Reticular Chemistry: Metal-Organic Frameworks and Covalent Organic Frameworks* (Wiley, 2019).
20. Diercks, C. S. & Yaghi, O. M. The atom, the molecule, and the covalent organic framework. *Science* **355**, eaal158 (2017).
21. Li, H., Dilipkumar, A., Abubakar, S. & Zhao, D. Covalent organic frameworks for CO_2 capture: from laboratory curiosity to industry implementation. *Chem. Soc. Rev.* **52**, 6294–6329 (2023).
22. Lyu, H., Li, H., Hanikel, N., Wang, K. & Yaghi, O. M. Covalent organic frameworks for carbon dioxide capture from air. *J. Am. Chem. Soc.* **144**, 12989–12995 (2022).
23. Lin, J.-B. et al. A scalable metal-organic framework as a durable physisorbent for carbon dioxide capture. *Science* **374**, 1464–1469 (2021).
24. Quang, D. V. et al. Effect of moisture on the heat capacity and the regeneration heat required for CO_2 capture process using PEI impregnated mesoporous precipitated silica. *Greenhouse Gases Sci. Technol.* **5**, 91–101 (2015).
25. Jin, E. et al. Two-dimensional sp^2 carbon–conjugated covalent organic frameworks. *Science* **357**, 673–676 (2017).
26. Lyu, H., Diercks, C. S., Zhu, C. & Yaghi, O. M. Porous crystalline olefin-linked covalent organic frameworks. *J. Am. Chem. Soc.* **141**, 6848–6852 (2019).
27. Pawley, G. S. Unit-cell refinement from powder diffraction scans. *J. Appl. Crystallogr.* **14**, 357–361 (1981).
28. Brunauer, S., Emmett, P. H. & Teller, E. Adsorption of gases in multimolecular layers. *J. Am. Chem. Soc.* **60**, 309–319 (1938).
29. Ji, W. et al. Removal of GenX and perfluorinated alkyl substances from water by amine-functionalized covalent organic frameworks. *J. Am. Chem. Soc.* **140**, 12677–12681 (2018).
30. Mao, H. et al. A scalable solid-state nanoporous network with atomic-level interaction design for carbon dioxide capture. *Sci. Adv.* **8**, eabo6849 (2022).
31. McCabe, W. L., Smith, J. C. & Harriott P. *Unit Operations of Chemical Engineering* 7th edn (McGraw Hill, 2004).
32. Panda, D., Kulkarni, V. & Singh, S. K. Evaluation of amine-based solid adsorbents for direct air capture: a critical review. *React. Chem. Eng.* **8**, 10–40 (2023).
33. Kolle, J. M., Fayaz, M. & Sayari, A. Understanding the effect of water on CO_2 adsorption. *Chem. Rev.* **121**, 7280–7345 (2021).
34. Ilkaeva, M. et al. Assessing CO_2 capture in porous sorbents via solid-state NMR-assisted adsorption techniques. *J. Am. Chem. Soc.* **145**, 8764–8769 (2023).

Publisher's note Springer Nature remains neutral with regard to jurisdictional claims in published maps and institutional affiliations.

Springer Nature or its licensor (e.g. a society or other partner) holds exclusive rights to this article under a publishing agreement with the author(s) or other rightsholder(s); author self-archiving of the accepted manuscript version of this article is solely governed by the terms of such publishing agreement and applicable law.

© The Author(s), under exclusive licence to Springer Nature Limited 2024

Methods

Synthesis of COF-999-N_3

A borosilicate glass tube measuring 8 × 10 mm (i.d. × o.d.) was charged with TCPB (16.9 mg, 0.04 mmol), BPDA-N_3 (29.6 mg, 0.06 mmol), Cs_2CO_3 (39.1 mg, 0.12 mmol), 1,2-dichlorobenzene (0.5 ml) and 1-butanol (0.5 ml). The mixture was flash frozen at 77 K in a liquid nitrogen bath, evacuated to an internal pressure below 0.2 mbar and then flame sealed. The length of the tube was reduced to around 10 cm on sealing. After warming to room temperature, the mixture was heated at 120 °C for 3 days in an oven to yield a yellow solid. The solid was filtered, washed with methanol (30 ml) and was used directly for the next step without further treatment. To characterize COF-999-N_3, the yellow solid described above was transferred into a tea bag and further washed with methanol for 16 h in a Soxhlet extractor, dried with supercritical CO_2 and degassed at 30 °C for 3 h under vacuum to yield COF-999-N_3 as a yellow solid (36 mg, yield 81%). Elemental analysis for $C_{23}H_{21}N_4O$: calculated C 74.77%, H 5.73%, N 15.17%; found C 74.08%, H 5.79%, N 14.01%.

Synthesis of COF-999-NH_2

To a 100-ml round bottom flask, COF-999-N_3 (100 mg), PPh_3 (200 mg) and 30 ml methanol were added under 25 °C. After 24 h, the suspension was filtered and washed with methanol to remove excess PPh_3. The yellow residue was transferred to another 100-ml round bottom flask, and 24 ml methanol and 6 ml water were added under 25 °C. After 24 h, the suspension was filtered into a tea bag, washed with methanol for 16 h in a Soxhlet extractor, dried with supercritical CO_2 and degassed at 30 °C for 3 h under vacuum to yield COF-999-NH_2 as a yellow solid (91 mg, yield 98%). Elemental analysis for $C_{23}H_{23}N_2O$: calculated C 80.44%, H 6.75%, N 8.16%; found C 78.51%, H 6.38%, N 8.10%.

Synthesis of COF-999

COF-999-NH_2 (30 mg), toluene (2 ml), acetic acid (5 µl) and aziridine (100 µl) were added to a borosilicate glass tube measuring 8 × 10 mm (i.d. × o.d.). The mixture was flash frozen at 77 K in a liquid nitrogen bath, evacuated to an internal pressure below 0.3 mbar and then flame sealed. The length of the tube was reduced to around 10 cm on sealing. After warming to room temperature, the reaction mixture was heated at 100 °C for 24 h. After cooling down to 25 °C, the solid was filtered into a tea bag, washed with 50 ml 1 M NaOH in methanol, then washed with methanol for 16 h in a Soxhlet extractor and dried at 120 °C for 12 h under vacuum to yield COF-999 as a yellow solid (36 mg, yield 86%). Elemental analysis for $C_{23}H_{23}N_2O{\cdot}(C_2H_5N)_{3.1}$: calculated C 73.53%, H 8.14%, N 14.98%; found C 70.19%, H 7.24%, N 14.35%.

Powder X-ray diffraction

PXRD patterns were collected using a Rigaku Miniflex 600 X-ray diffractometer in reflection geometry using Cu Kα radiation (λ = 1.54184 Å, with an Ni filter) at a power of 600 W (40 kV, 15 mA). Samples were mounted on Si (511) sample holders and levelled with a spatula. The step size was 0.02° with an exposure time of 0.5 s per step.

Solid-state nuclear magnetic resonance spectroscopy

Solid-state NMR experiments were conducted at an external field B_0 = 16.4 T (700 MHz for ^{1}H, 176 MHz for ^{13}C and 71 MHz for ^{15}N) using a Bruker Avance I spectrometer and a 3.2-mm H/C/N magic-angle spinning (MAS) probe. To reduce CO_2 and moisture exposure, COF samples were fully activated, then packed in 3.2 mm zirconia rotors and closed using Vespel caps in an argon-filled glovebox. $^{13}CO_2$-dosed COF samples were conducted by exposing dry or pre-humidified (by N_2 with 80% RH) COF-999 samples to 1 atm $^{13}CO_2$ gas (2.47 atm, Sigma Aldrich, 99% atom ^{13}C) for 3 h at room temperature, followed by evacuation (<0.3 mbar) at room temperature to remove excess CO_2. Unless specified differently, ^{13}C and ^{15}N experiments were performed under MAS at a spinning rate of 23 kHz and 11 kHz using dry air, respectively. ^{13}C chemical shifts were externally referenced using the tertiary carbon (CH) resonance of adamantane at 38.48 ppm. ^{15}N chemical shifts were externally referenced to ^{15}N-glycine at 33.4 ppm.

^{15}N spectra of COF-999-$^{15}N_3$ and COF-999-$^{15}NH_2$ were obtained using ^{1}H → ^{15}N cross-polarization under MAS (CP-MAS). After an initial ^{1}H 90° radiofrequency pulse of 5.20 µs (48.1 kHz), a CP transfer contact time of 2 ms was used, during which a constant radiofrequency field equal to 25.3 kHz was applied on ^{15}N, whereas the ^{1}H radiofrequency-field amplitude was linearly ramped from 43.3 kHz to 48.1 kHz. During ^{15}N acquisition, high-power ^{1}H decoupling was applied using the SPINAL-64 (Small Phase Incremental Alternation with 64 steps) decoupling scheme[35] with a radiofrequency-field amplitude set to 48.1 kHz. For COF-999-$^{15}N_3$, a total of 30,688 scans were recorded with a recovery delay of 2 s, leading to an overall experimental time of 17 h. For COF-999-$^{15}NH_2$, a total of 896 scans were recorded with a recovery delay of 2.23 s, leading to an overall experimental time of 34 min.

Quantitative ^{15}N spectra of ^{15}N labelled COF-999 were obtained using multiple CP transfers as described in ref. 36. For each scan, a total of four CP transfers were used to saturate the ^{15}N signals of COF-999, with an initial recovery delay of 7.28 s ($5 \times T_1(^1H)$) and a delay of 2.91 s ($2 \times T_1(^1H)$) in between CP transfers. The ^{1}H → ^{15}N CP transfer used the same parameters described previously and in total, 1,088 scans were averaged, leading to an overall experimental time of 6 h.

^{13}C spectra of COF-999-N_3 were obtained using ^{1}H → ^{13}C CP-MAS. After an initial ^{1}H 90° radiofrequency pulse of 5.20 µs (48.1 kHz), a CP transfer contact time of 2 ms was used, during which a constant radiofrequency field equal to 34.5 kHz was applied on ^{13}C, whereas the ^{1}H radiofrequency-field amplitude was linearly ramped from 43.3 kHz to 48.1 kHz. During ^{13}C acquisition, high-power ^{1}H decoupling was applied using the SPINAL-64 decoupling scheme with a radiofrequency-field amplitude set to 48.1 kHz. A total of 9,856 scans were recorded with a recovery delay of 1.3 s, leading to an overall experimental time of 3.6 h.

Quantitative ^{13}C spectra of COF-999-NH_2 and COF-999 were obtained using multiple CP transfers. For each scan, a total of 10 or 14 CP transfers were used to saturate the ^{13}C signals of COF-999-NH_2 or COF-999, respectively, with an initial recovery delay of 5 s or 4.25 s and a delay of 2 s or 1.71 s in between CP transfers. The ^{1}H → ^{13}C CP transfer used the same parameters described previously and in total, 1,940 or 3,833 scans were averaged, leading to overall experimental times of 14 h or 30 h for COF-999-NH_2 or COF-999, respectively.

Direct excitation experiments of $^{13}CO_2$-dosed COF-999 were performed under MAS at 10 kHz with a 90° pulse of 4.12 µs. During ^{13}C acquisition, high-power ^{1}H decoupling was applied using the SPINAL-64 decoupling scheme with a radiofrequency-field amplitude set to 48.1 kHz. In total, 64 scans were averaged with a recycle delay of 120 s, leading to an experimental time of 2.2 h.

Single-component sorption isotherm measurements

N_2 sorption isotherms at 77 K were measured using a Micromeritics ASAP 2420 (Accelerated Surface Area and Porosimetry) System. Powder samples were activated under a dynamic vacuum using a Micromeritics ASAP 2420 System before measurement. A liquid nitrogen bath was used to maintain a temperature of 77 K for each measurement. Ultrahigh-purity N_2 (Praxair, 99.999%) and He (Praxair, 99.999%) gases were used throughout the adsorption experiments.

CO_2 sorption isotherms were measured using a Micromeritics 3Flex Adsorption Analyser. Powder samples were activated under a dynamic vacuum using a Micromeritics ASAP 2420 System before measurement. A water circulation bath was used to maintain the temperature during the measurements. Research-grade CO_2 (Praxair, 99.998%) was used throughout the adsorption experiments.

O_2, N_2 and Ar sorption isotherms at 25 °C were measured using a 3P micro 200 analysis station. Powder samples were activated by the activation station of 3P micro 200 before measurement. A cryoTune 195 was used to maintain a temperature of 25.00 °C for each measurement.

Research-grade O_2 (TIG, 99.995%) and research-grade N_2 (TIG, 99.999%) were used throughout the adsorption experiments.

H_2O vapour sorption experiments were carried out on a Belsorp MAX II high-precision gas and vapour adsorption measurement instrument. Powder samples were activated under a dynamic vacuum using Belprep VAC III before measurement. The water vapour source was degassed through five freeze–pump–thaw cycles before the analysis. Ultrahigh-purity He (Praxair, 99.999%) was used for free space corrections, and an isothermal bath was used to adjust the sample temperature during the measurements.

Dynamic breakthrough measurements

Dynamic breakthrough experiments were carried out on a Micromeritics Breakthrough Analyser equipped with a CO_2 sensor (detection range: 0.6–984.9 ppm) and a humidity sensor. The samples were packed in a jacked column (4.9 mm i.d.) and the temperature was controlled by a Ministat 230 oil circulation bath. Ultrahigh-purity N_2 (Praxair, 99.999%), research-grade CO_2 (Praxair, 99.998%), ultra-zero-grade air (Praxair), 1,000 ppm CO_2 balanced in air (Praxair), 1% CO_2 balanced in N_2 (Praxair) and 20% CO_2 balanced in N_2 (Praxair) were used for breakthrough measurements.

The humidified air or N_2 can be obtained by passing the dry air or N_2 through a water bath. Different CO_2 concentrations and relative humidities can be fine-tuned by adjusting the blend ratio of different gases. Specifically, 400 ppm CO_2 balanced in air was mixed by humid air, dry air, and 1,000 ppm CO_2 balanced in air; 400 ppm CO_2 balanced in N_2 was mixed by humid N_2, dry N_2 and 1% CO_2 balanced in N_2; 4% CO_2 balanced in N_2 was mixed by humid N_2, dry N_2 and 20% CO_2 balanced in N_2; 15% CO_2 balanced in N_2 was mixed by humid N_2, dry N_2 and pure CO_2.

Ambient air was collected from the sixth-floor (room 626) balcony of Latimer Hall, Berkeley, California, United States (37° 52′ 23.8″ N 122° 15′ 21.2″ W) between 18 January 2024 and 6 February 2024. The ambient air was pressurized by a Welch 2522B-01 dry pump to 300 kPa and was then stabilized at 200 kPa by an Aldrich HPL500-2160 mini gas regulator before being introduced into the breakthrough analyser.

In the adsorption capacity measurements, 90–280 mg of COF-999 sample was packed in the jacked column. The oil bath was first heated to 80 °C, resulting in a column wall temperature of 76 °C and a column centre temperature of 48 °C. A 50 sccm N_2 flow was passed through the sample until the outlet CO_2 concentration was less than 5 ppm. Then, the oil bath was cooled and maintained at 25 °C, and the sample was exposed to 10 sccm or 50 sccm simulated gas mixture with desired CO_2 concentration (400 ppm, 4.0% or 15.0%) balanced in N_2 with desired RH (0%, 25%, 50% or 75%) until the outlet CO_2 concentration was constant. The specific CO_2 uptake of the sample was then obtained as the difference between the apparent and background uptakes per unit mass of the sample.

In the cycling stability measurements, 80 mg of COF-999 sample was packed in the jacked column. The oil bath was first heated to 64 °C, resulting in a column wall temperature of 60 °C and a column centre temperature of 41 °C. A 50 sccm N_2 flow was passed through the sample until the outlet CO_2 concentration was less than 5 ppm. Then, the oil bath was cooled and maintained at 25 °C, and the sample was exposed to 50 sccm 400 ppm of CO_2 balanced in air with 50% RH until the outlet CO_2 concentration was higher than 395 ppm. The sample was reactivated through the same procedure described above before each cycle. The specific CO_2 uptake of the sample was then obtained as the difference between the apparent and background uptakes per unit mass of the sample.

In the adsorption kinetics measurements, 5.0 mg of COF-999 sample was packed in the jacked column. The oil bath was first heated to 80 °C, resulting in a column wall temperature of 76 °C and a column centre temperature of 48 °C. A 50 sccm N_2 flow was passed through the sample for 120 min to fully activate the sample. Then, the oil bath was cooled and maintained at 25 °C, and the sample was humidified by exposing it to 50 sccm CO_2-free air with 50% RH for 30 min, followed by 50 sccm 400 ppm CO_2 balanced in air with 50% RH until the outlet CO_2 concentration was constant. The specific CO_2 uptake of the sample was then obtained as the difference between the apparent and background uptakes per unit mass of the sample.

In the desorption kinetics measurements, 5.0 mg of COF-999 sample was packed in the jacked column. The sample was first exposed to 50 sccm 400 ppm CO_2 balanced in air with 50% RH until the outlet CO_2 concentration was constant. Then, the column was heated under 50 sccm N_2 flow until the column wall temperature reached 60 °C, 80 °C or 100 °C. The column temperature was maintained for 3 h for desorption. The amount of desorbed CO_2 was obtained as the integrated downstream CO_2 concentration per unit mass of the sample.

In the outdoor air capture experiments, 73 mg of COF-999 sample was packed in the jacked column. For each cycle, the oil bath was first heated to 64 °C, resulting in a column wall temperature of 60 °C and a column centre temperature of 41 °C. A 50 sccm N_2 flow was passed through the sample until the outlet CO_2 concentration was less than 20 ppm (typically 90 min). Then, the oil bath was cooled to 25 °C and turned off. Background RH and CO_2 concentration of the outdoor air were measured through the bypass (at around 25 °C). The sample was then exposed to 50 sccm ambient air until the outlet CO_2 concentration was higher than 300 ppm. The sample was reactivated through the same procedure described above before each cycle. The specific CO_2 uptake of the sample was then obtained as the difference between the apparent and background uptakes per unit mass of the sample. Adsorption capacity measurements were conducted before and after the outdoor air capture experiments using simulated air (400 ppm of CO_2 with 50% RH) to assess the stability of the sample.

Periodic density functional theory calculations

Density functional theory (DFT) calculations were performed in the Vienna Ab Initio Simulation (VASP v.6.1) software[37–39] to investigate CO_2 adsorption in COF-999. The Perdew–Burke–Ernzerhof (PBE) exchange-correlation density functional[40] was used along with the D3 dispersion corrections of Grimme with Becke–Johnson damping (PBE-D3BJ)[41] for all the calculations. Generally, for the structural optimization of each adsorbed species in COF-999, a plane-wave basis set with an energy cutoff of 400 eV was used. Each structure was optimized until the energy and force convergence criteria of 10^{-6} eV and 0.03 eV $Å^{-1}$ were achieved. A $1 \times 1 \times 3$ Γ-centred k-point grid was used for the Brillouin zone sampling. During each structural optimization, only the atom positions were relaxed while the unit cell parameters were held constant.

A structural model for COF-999 was obtained from the COF-999-NH_2 structure. First, the structure of COF-999-NH_2 was optimized using DFT with the following settings. The PBE-D3BJ exchange-correlation density functional with dispersion corrections and a plane-wave basis set with an energy cutoff of 520 eV were used. The same energy and force convergence criteria as described above were used, whereas a $1 \times 1 \times 5$ Γ-centred k-point grid was used for the Brillouin zone sampling. A higher energy cutoff and denser k-point grids were used for the initial optimization of COF-999-NH_2 as compared with subsequent structure optimizations of COF-999 because the positions of the atoms as well as unit cell parameters were relaxed during the structure optimization. The optimized COF-999-NH_2 structure was then modified to introduce 4.5 $-CH_2-CH_2-NH-$ units (on average) with branching on two out of the six sidechains in COF-999-NH_2. This model is representative of the polymeric polyethyleneimine units formed in COF-999 and encompasses the varied CO_2 adsorption sites constituted by primary, secondary and tertiary amines. This optimized structure (unit cell parameters: $a = b = 45.084$ Å, $c = 3.819$ Å, $\alpha = \beta = 90°$ and $\gamma = 120°$) was used for investigating CO_2 adsorption in COF-999. Owing to the conformational flexibility of the polyamine chains, we investigated several different CO_2 adsorption environments constituted by polyamines

and representative of these are shown here. The adsorption energy, $\Delta E_{\text{adsorption}}$, (electronic energy) was calculated using

$$\Delta E_{\text{adsorption}} = E_{\text{adsorbed system}} - E_{\text{empty COF}} - n_{CO_2} \times E_{\text{isolated } CO_2} - n_{H_2O} \times E_{\text{isolated } H_2O} \quad (1)$$

where $E_{\text{adsorbed system}}$ is the electronic energy of the system on adsorption, $E_{\text{empty COF}}$ is the electronic energy of the empty COF having a similar conformation of the polyamines as in the adsorbed state, $E_{\text{isolated } CO_2}$ and $E_{\text{isolated } H_2O}$ are the electronic energies of an isolated CO_2 and H_2O molecule, respectively, and n_{CO_2} and n_{H_2O} are the number of adsorbed CO_2 and H_2O molecules.

Data availability

All experimental data are available in the main text or Supplementary Information. Computational results are available on Zenodo (https://doi.org/10.5281/zenodo.13382234) (ref. 42). Source data are provided with this paper.

35. Fung, B. M., Khitrin, A. K. & Ermolaev, K. An improved broadband decoupling sequence for liquid crystals and solids. *J. Magn. Reson.* **142**, 97–101 (2000).
36. Johnson, R. L. & Schmidt-Rohr, K. Quantitative solid-state ^{13}C NMR with signal enhancement by multiple cross polarization. *J. Magn. Reson.* **239**, 44–49 (2014).
37. Kresse, G. & Hafner, J. *Ab initio* molecular dynamics for liquid metals. *Phys. Rev. B* **47**, 558–561 (1993).
38. Kresse, G. & Furthmüller, J. Efficiency of ab-initio total energy calculations for metals and semiconductors using a plane-wave basis set. *Comput. Mater. Sci.* **6**, 15–50 (1996).
39. Kresse, G. & Furthmüller, J. Efficient iterative schemes for *ab initio* total-energy calculations using a plane-wave basis set. *Phys. Rev. B* **54**, 11169–11186 (1996).
40. Perdew, J. P., Burke, K. & Ernzerhof, M. Generalized gradient approximation made simple. *Phys. Rev. Lett.* **77**, 3865–3868 (1996).
41. Grimme, S., Ehrlich, S. & Goerigk, L. Effect of the damping function in dispersion corrected density functional theory. *J. Comput. Chem.* **32**, 1456–1465 (2011).
42. Zhou, Z. et al. Computational results for the publication "Carbon dioxide capture from open air using covalent organic frameworks". Zenodo https://doi.org/10.5281/zenodo.13382234 (2024).

Acknowledgements Z.Z. thanks H. Lyu, O. I.-F. Chen, Z. Rong and W. Xu (Yaghi Research Group, UC Berkeley) for their discussions. We thank H. Celik and the Core NMR Facility of UC Berkeley Pines Magnetic Resonance Center for spectroscopic assistance. We also thank the UC Berkeley Electron Microscope Laboratory for access and assistance in electron microscopy data collection. This research was supported by the King Abdulaziz City for Science and Technology (Center of Excellence for Nanomaterials and Clean Energy Applications), ATOCO and the Bakar Institute of Digital Materials for the Planet. The NMR instruments used in this work were supported by the National Science Foundation under grant no. 2018784 and by the National Institutes of Health under grant S10OD024998. Z.Z. and O.M.Y. acknowledge the interest and support of Fifth Generation (Love, Tito's). S.E. thanks the Free State of Saxony and the European Union (Low Surface and Pore Sorption LSPS) for financial support. J.S. is also a distinguished visiting scholar at UC Berkeley.

Author contributions Z.Z. and O.M.Y. conceived the idea and led the experimental efforts. Z.Z. designed the COFs and developed synthetic methodologies. Z.Z., T.M., H.Z. and C.L. conducted the synthesis of linkers and COF-999-N_3. T.M. and Z.Z. collected and analysed the SEM, PXRD, thermogravimetric analysis and FT-IR data. Z.Z., R.G. and K.W. conducted the NMR experiments. Z.Z., K.W., T.M., S.E. and A.H.A. collected the gas sorption data. Z.Z., H.L. and S.E. performed the breakthrough experiments. S.C. and J.S. led the computational analysis. S.C. conducted the DFT calculations. L.G. advised on the computational setup. M.M.A. and M.O.A. provided valuable suggestions throughout this study. Z.Z., T.M. and O.M.Y. prepared the initial draft and finalized it. All authors contributed to revising the paper.

Competing interests COF-999 and its related materials have been filed as US Provisional Patent Application no. 63/587,185 by UC Berkeley. O.M.Y. and Z.Z. are the inventors of this patent. O.M.Y. is a co-founder of ATOCO, aiming at commercializing related technologies. The other authors declare no competing interests.

Additional information

Supplementary information The online version contains supplementary material available at https://doi.org/10.1038/s41586-024-08080-x.

Correspondence and requests for materials should be addressed to Joachim Sauer or Omar M. Yaghi.

Peer review information *Nature* thanks the anonymous reviewers for their contribution to the peer review of this work. Peer reviewer reports are available.

Reprints and permissions information is available at http://www.nature.com/reprints.

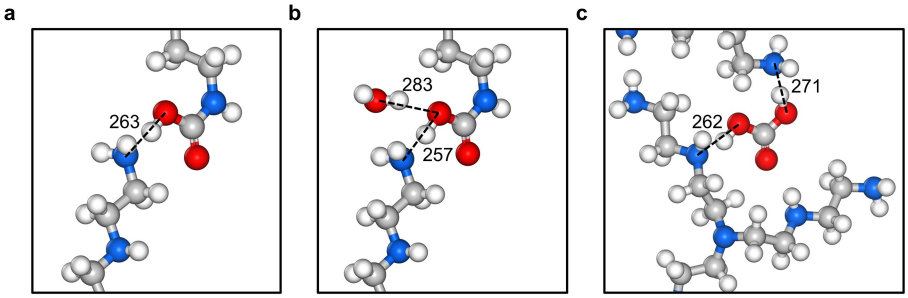

Extended Data Fig. 1 | CO_2 adsorption structures in COF-999. a, Formation of carbamic acid under dry conditions. **b**, Formation of carbamic acid/carbamate under humid conditions. **c**, Formation of bicarbonate under humid conditions. All numbers represent atom distances in pm. C, gray; N, blue; O, red; H, white. Additional structures are shown in Supplementary Information section 14.